AIP Advances CELEBRATING 5 YEARS

A half-metallic half-Heusler alloy having the largest atomic-like magnetic moment at optimized lattice constant

R. L. Zhang, L. Damewood, C. Y. Fong, L. H. Yang, R. W. Peng, and C. Felser

Citation: AIP Advances **6**, 115209 (2016); doi: 10.1063/1.4967365
View online: http://dx.doi.org/10.1063/1.4967365
View Table of Contents: http://scitation.aip.org/content/aip/journal/adva/6/11?ver=pdfcov
Published by the AIP Publishing

Articles you may be interested in

Anisotropy in layered half-metallic Heusler alloy superlattices
J. Appl. Phys. **119**, 043904 (2016); 10.1063/1.4940878

The realization of ferro-ferrimagnetic transition and half-metallicity in half-Heusler CoMnGa alloy
Appl. Phys. Lett. **105**, 212403 (2014); 10.1063/1.4902523

Ground state study of half-metallic ferromagnetism in the half-Heusler compound Gekca using density functional theory
AIP Conf. Proc. **1536**, 1047 (2013); 10.1063/1.4810593

First principle prediction of half-metallic ferromagnetism above room temperature in half-heusler alloys
AIP Conf. Proc. **1199**, 441 (2010); 10.1063/1.3295495

Magnetic and half-metallic properties of the full-Heusler alloys Co 2 Ti X (X = Al , Ga ; Si , Ge , Sn ; Sb)
J. Appl. Phys. **97**, 10C307 (2005); 10.1063/1.1853899

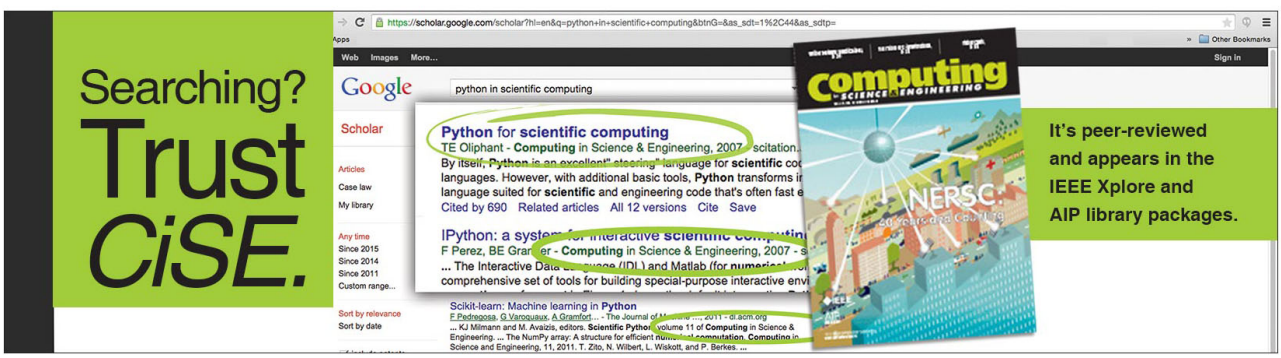

Reuse of AIP Publishing content is subject to the terms at: https://publishing.aip.org/authors/rights-and-permissions. Download to IP: 210.28.138.101 On: Wed, 09 Nov 2016 09:23:29

A half-metallic half-Heusler alloy having the largest atomic-like magnetic moment at optimized lattice constant

R. L. Zhang,[1,2,a] L. Damewood,[2] C. Y. Fong,[2] L. H. Yang,[3] R. W. Peng,[1] and C. Felser[4]

[1]*School of Physics and Collaborative Innovation Center of Advanced Microstructures, Nanjing University, Nanjing 210093, China*
[2]*Department of Physics, University of California, Davis, California 95616-8677, USA*
[3]*Physics Division, Lawrence Livermore National Laboratory, Livermore, California 94551, USA*
[4]*Institut für Anorganische Chemie und Analytische Chemie, Johannes Gutenberg-Universität Mainz, 55099 Mainz, Germany*

(Received 12 August 2015; accepted 26 October 2016; published online 2 November 2016)

For half-Heusler alloys, the general formula is XYZ, where X can be a transition or alkali metal element, Y is another transition metal element, typically Mn or Cr, and Z is a group IV element or a pnicitide. The atomic arrangements within a unit-cell show three configurations. Before this study, most of the predictions of half-metallic properties of half-Heusler alloys at the lattice constants differing from their optimized lattice constant. Based on the electropositivity of X and electronegativity of Z for half-Heusler alloys, we found that one of the configurations of LiCrS exhibits half-metallic properties at its optimized lattice constant of 5.803Å, and has the maximum atomic-like magnetic moment of $5\mu_B$. The challenges of its growth and the effects of the spin-orbit effect in this alloy will be discussed. © *2016 Author(s). All article content, except where otherwise noted, is licensed under a Creative Commons Attribution (CC BY) license (http://creativecommons.org/licenses/by/4.0/).* [http://dx.doi.org/10.1063/1.4967365]

Since the prediction of half-metallic properties in the half-Heusler of NiMnSb by de Groot *et al.*,[1] much attention has been paid exploring half-metallic half-Heusler alloys for device applications.[2,3] In half-metals (HM), one spin channel is metallic while the other channel is insulating. Thus, the density of states (DOS) of a HM at the Fermi energy, E_F, is contributed entirely by states of one spin channel. Consequently, the spin polarization can achieve 100%. This characteristic offers exciting and unique opportunities for the occurrence of infinite magnetoresistance as predicted by the Julliére formula.[4]

Heusler alloys have been well studied. The formula characterizing half- Heusler alloys is XYZ where X can be an alkali metal element or a transition metal element, TME, such as Ni in NiMnSb. Y is another TME and Z is either a group IV or a group V element. These alloys have the $C1_b$ crystal structure, which is similar to the $L2_1$ structure of a full-Heusler alloy (X_2YZ) except missing one X to form a vacancy.[5] There are three possible atomic arrangements for the XYZ in a unit cell, i.e. ZXY, YZX, and XYZ, and we call them α, β, and γ configurations, respectively. The positions of the three atoms, X, Y and Z for each configuration are listed in Table I according to the notation defined by Wyckoff.[6] Fig. 1 shows the $C1_b$ structure. Many of half-Heusler alloys have been predicted to be half-metals[7,8] with lattice constants deviating away (mostly larger) from the optimized lattice constants. For example, Damewood *et al.* examined half-metallic properties and stability of lithiated half-Heusler alloys, LiMnZ (Z=N, P, Si).[8] They found that the studied alloy exhibit half-metallic properties at lattice constants larger than its' optimized lattice constant. In fact, many zinc-blende (ZB) compounds, such as MnZ, are not half-metallic at their equilibrium lattice constants but can also

[a]To whom correspondence should be addressed. E-mail address: rlzhang@nju.edu.cn.

 © Author(s) 2016

Reuse of AIP Publishing content is subject to the terms at: https://publishing.aip.org/authors/rights-and-permissions. Download to IP: 210.28.138.101 On: Wed, 09 Nov 2016 09:23:29

TABLE I. The positions of the three atoms, X, Y and Z, and the vacancy in terms of the Wyckoff notation: 4a=(0,0,0)a_0, 4b=(1/2,1/2,1/2)a_0, 4c=(1/4,1/4,1/4)a_0 and 4d=(1/4,3/4,1/4)a_0 (not appeared in the table. It is a vacancy), where a_0 is the lattice parameter. The zinc blende structure, YZ, is included for comparison.

Structure	Element position		
	X	Y	Z
α	4c	4b	4a
β	4b	4a	4c
γ	4a	4c	4b
Zinc blende		4a	4c

be HMs at larger lattice constants.[9] Akinaga *et al.* argued that strained materials are tolerable because it is possible to grow them in thin film forms on substrates, such as CrAs grown on GaAs.[10] However, it is a common sense to expect that devices using strained materials will not have a long life-time. In order to have a long lived device, the material should at least be metastable. For half-Heusler alloys, the better ones used for device materials should at least be at the optimized lattice constants corresponding to their respective configurations. Furthermore, a large magnetic moment (>3 μ_B) can lead to the Curie temperature, T_C, above room temperature.[11] Consequently, can the half-metallic Heusler alloys exhibit the largest or even atomic magnetic moments contributed by the 3d-states of the TME?

In this paper, we address the following issue: is it possible to find a configuration of a half-metallic half-Heusler alloy possessing the largest atomic-like magnetic moment, 5 μ_B, at an optimized lattice constant so that devices made of the alloy not only can have high T_C but also do not suffer large strains for making a long life time spintronic device? Instead of carrying out experimental search, we use the common practice of utilizing spin polarized first principles calculations to predict the possibility.

Shaughnessy *et al.*[12] suggested a point of view in half-Heusler alloys unifying the d-p and d-d bonding based on the 'electronegativity'. In these alloys, Z is the most electronegative among the three atoms. So, it should be possible for Z to form a d-p bonding with its nearest neighbor (nn) and determine the primary gap: the bonding-antibonding gap. If there are two TME in an alloy, weak bonds between the two TME form the d-d bonding states and contribute to the states near E_F resulting in a much smaller gap. By combining the concept of "electropositivity", results of Li-based half-Heusler alloys in β-LiMnZ with pinictide Z, the nearest neighbor to both Li and Mn, are understood. Li is the most electropositive among the three atoms and easily gives up its outermost electron to its neighbor. The most electronegative Z atom gains an electron from Li. To fill its p-shell, Z takes additional two s-electrons from Mn since they are nn pair. The five remaining d-electrons at the Mn form local magnetic moment of 5 μ_B per Mn. If Z is a group IV element, then the moment is 4 μ_B per Mn.[8] However, the lattice constants are consistently larger than the optimized values. This may be caused by the fact that the pnictides and Si do not have a sufficiently strong enough electronegativity. The residual covalent character between the bonds formed by the TME and Z do not provide enough of a large volume in order to align their spins. If this explanation is true, we should try to use elements at the right side of the pnictides in the periodic table. A new physical condition appears. Any element

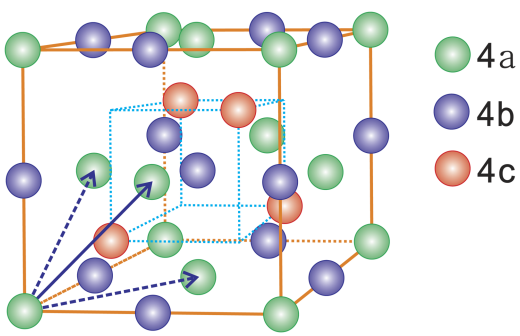

FIG. 1. Diagrammatic sketch of $C1_b$ structure.

Reuse of AIP Publishing content is subject to the terms at: https://publishing.aip.org/authors/rights-and-permissions. Download to IP: 210.28.138.101 On: Wed, 09 Nov 2016 09:23:29

TABLE II. The optimized lattice constants, total energies, and magnetic moments for three configurations of LiSCr alloys.

Compounds	Lattice constant(Å)	Total energy(eV)	Magnetic moment (μ_B/Mn)
α - LiCrS	5.803	-15.652	5.0000
β - LiCrS	5.795	-16.663	4.4548
γ - LiCrS	5.923	-15.948	4.9385

at one column right of the pnictides in the periodic table needs only two electrons to fill its outer valence shell. Mn should be replaced by TME of valence 6 for achieving the largest magnetic moment – the d-shell is half filled. In the following, we report on first principles results of LiCrS meeting the expectation.

The spin-polarized version of VASP[13,14] was used for the calculations. The VASP package provides projector-augmented-wave (PAW) pseudopotentials[15] for Li, Cr, and S that were constructed by using the generalized gradient approximation (GGA) of Perdew *et al.* (PBE).[16] The GGA was also used to treat the exchange-correlation between electrons in the crystal calculations. We used the basis of plane waves with a 1000 eV kinetic energy cutoff for all calculations. The Monkhorst–Pack mesh of (15, 15, 15) was adopted to calculate the total charge density.

In Table II, the lattice constants of the primitive cell, the total energies, and the magnetic moments of α , β , and γ-LiCrS are presented. The α configuration has the moment of 5 μ_B at its optimized lattice constant. It is the first case having this unique feature and in fact it has a range of the lattice constants (5.8 – 5.83 Å) to have the total energy of -15.650 eV and moment of 5 μ_B. We present the total density of states (DOS) for α- and β-LiCrS at their optimized lattice constants 5.803Å and 5.795Å in Figs. 2(a) and 2(c), respectively. The DOS for the γ configuration is not shown because it exhibits a very similar result to the β configuration, because in both cases, Cr and S are nearest neighbors (nn), and the position of Li atom does not drastically alter the DOS. As shown in Figs. 2(a) and 2(c), the gap of spin down channel for α-LiCrS is well defined, while there are states of spin down channel for β-LiCrS overlapping with the states of spin up channel at the Fermi level. Therefore, α-LiCrS demonstrates the half-metal (HM) property, while β configuration is not a half metal at its optimized lattice constant. Based on Julliére formula,[4] the spin polarization of α-LiCrS should be 100% at the Fermi level. However, the actual situation including the surface reconstruction, finite-temperature effects, etc. may lead to the deviation from the theoretical predictions.

In order to understand the states contributing to the gap in α-LiCrS, we plot the partial DOS of the so-called e_g (doubly degenerate d_{z^2} and $d_{x^2-y^2}$) and t_{2g} (triply degenerate d_{xy}, d_{yz} and d_{zx}) states of Cr, and p (i.e., p_x, p_y and p_z) states of S in the α and β configurations, respectively [Figs. 2(b) and 2(d)].

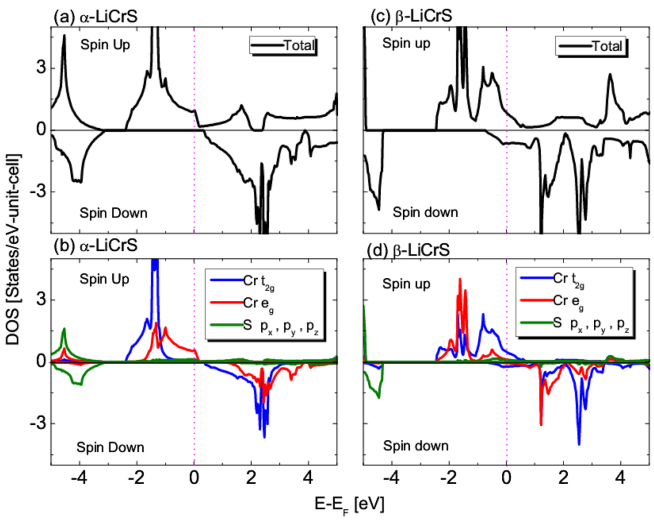

FIG. 2. The charge densities of LiCrS in the three configurations at their optimized lattice constants, respectively.

Reuse of AIP Publishing content is subject to the terms at: https://publishing.aip.org/authors/rights-and-permissions. Download to IP: 210.28.138.101 On: Wed, 09 Nov 2016 09:23:29

In the β configuration, there is a large gap for the spin down channel even though the E_F doesn't fall within it [Fig. 2(d)]. The valence band is contributed by the t_{2g} states of Cr and by significant p states of S. They form the bonding part of the bonding-antibonding gap due to hybridization of the t_{2g} states of Cr and sp^3 states of S under the tetrahedral environment. However, the α configuration is significantly different compared to the β configuration. From Fig. 2(b), the gap of the minority spin channel appears between the p states of S and the d states of Cr. The valence band is contributed primarily by the p states of S. In the α configuration, Cr and S are second neighbors. It's hard to form a bonding-antibonding gap coming from the hybridization of the d states of Cr and the sp^3 states of S. We attribute the gap of minority spin channel to the large electronegativity of the S atom to hold closer the transferred electrons from the nn Li and the second neighbor Cr leading to a large enough volume around the Cr to align its remaining five d-electrons governed by the Pauli principle. Consequently, the largest atomic-like magnetic moment 5 μ_B around Cr in α-LiCrS is obtained.

To confirm our attribution, we demonstrated the spin up ($\rho_\uparrow$), spin down ($\rho_\downarrow$), total ($\rho_\uparrow + \rho_\downarrow$), and spin polarized ($\rho_\uparrow - \rho_\downarrow$) charge density distributions for α-LiCrS at the optimized lattice constant in Figs. 3(a), 3(b), 3(c), and 3(d), respectively. It is found that the charge density approaches zero around Li, and presents small amplitude around S both for spin up and spin down electrons [Figs. 3(a) and 3(b)]. However, the charge density around Cr demonstrates large amplitude for spin up electrons [Fig. 3(a)], and is close to zero for spin down electrons [Fig. 3(b)]. As a result, the total charge density is strong around Cr and S, and near zero around Li [Fig. 3(c)], while the spin-polarized charge density is strong around Cr, and approximately zero around S and Li [Fig. 3(d)]. This feature comes from the fact that Li gives up its electron to the most electronegative element S. However, S needs another electron to fill its 3p orbit, and it captured the electron from Cr. For Cr, the normal electronic configurations are $(3d)^5(4s)^1$. It becomes $(3d)^5$ when it losses an electron. The five electrons align the same direction due to the intra-atomic exchange interaction.

It is worthwhile to compare the bonding features of α and β configurations. Figs. 4(a) and 4(b) show the contours of charge density for α and β-LiCrS at their optimized lattice constants,

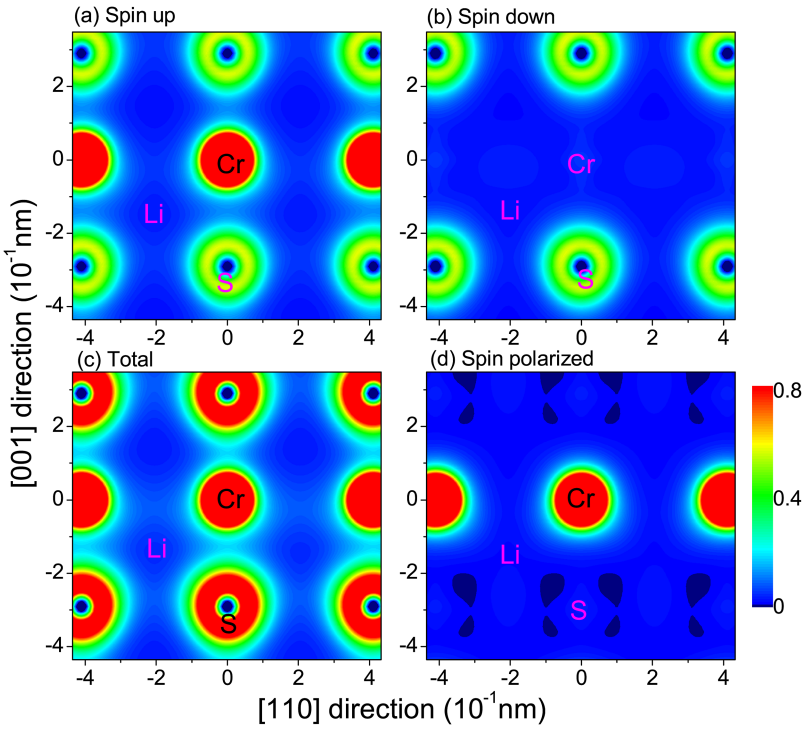

FIG. 3. Charge density distribution of α-LiCrS at the optimized lattice constant. The letters Cr, S, and Li are used to help reader find the atoms.

Reuse of AIP Publishing content is subject to the terms at: https://publishing.aip.org/authors/rights-and-permissions. Download to IP: 210.28.138.101 On: Wed, 09 Nov 2016 09:23:29

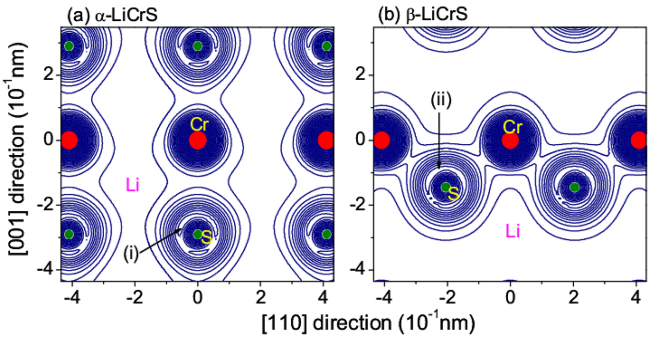

FIG. 4. The contours of charge density of (a) α-LiCrS, (b) β-LiCrS at their optimized lattice constants, respectively. In the red regions, the amplitude of charge density is larger than the other place, while in the olive regions the amplitude of charge density is smaller than the other place. Arrows (i) and (ii) point to bound charges near the S atoms. The letters Cr, S, and Li are used to help reader find the atoms.

respectively. It is clear that there is essentially no charge around the Li atoms both in α and β configurations because Li atoms contribute their electrons to the S atoms. The large electronegativity of S causes the bond charge to be located close to the S atom, denoted by the arrows (i) and (ii) in the Figs. 4(a) and 4(b), respectively. However, the contours of bond charge in regions (i) for the α configuration and (ii) for the β configuration are different. In region (i), the lobe exhibits less directional feature indicated by a roughly uniform width of the contour defining (i). In this α-LiCrS, Cr and S atoms are the second neighbors, and the large distance between them hindered the formation the covalent bond. In region (ii) the lobe directs the Cr atoms as demonstrated by slightly width change of the contour. The bonding feature for β configuration differs greatly from the one in α configuration because Cr and S atoms are nearest neighbors in the β-LiCrS. It becomes easy to form the covalent bond between them.

As to why the β-LiCrS is not a half-metal at its optimized lattice constant. We suggest the following explanations. The β configuration, in principle, would be the best candidate to resolve our issue because it has the lowest total energy. However, the Cr and S form nn pair. Their separation is smaller than the corresponding one in the α configuration. Thus, the S atom takes one electron each from its two nn. It does not leave enough space of the remaining five electrons at Cr to align their spins.

Table II indicates that the lattice constants of α and β configurations are very close. This can possibly present a challenge for the growth of α configuration. One may use a quenching scheme to grow the α configuration at a lattice constant larger than 5.79 Å based on the fact that it has a range of lattice constants (5.803 to 5.83 Å) with the total energy between -15.649 and -15.652 eV. Another issue is the spin-orbit effect for the α configuration. We found that with the spin-orbit interaction, the moment is changed to 4.9993 from . The spin-orbit effect is not negligible. This issue needs further study because there are s- and p-states at E_F and the gap states from the S atom. The situation differs from the ones studied in Ref. 17 where the states at E_F are d-like.

In conclusion, we predict using first-principles calculations that the α configuration of LiCrS exhibits a favorable property for long life time spintronic applications. It shows a large gap (3.26 eV), the largest atomic-like magnetic moment at its optimized lattice constant. There are remaining challenging issues, such as, the growth and the effect of the spin-orbit interaction. In our system, we only studied the collinear magnetization. The noncollinear magnetization can affect the demonstration of half-metallicity. Generally, the compounds that include Mn may exhibit noncollinear magnetic behaviour. Noncollinear magnetism can also originate from the geometric frustration or magnetic anisotropy. One can try to keep away from the above conditions to avoid the emergence of noncollinear magnetization.

This work was supported by grants from the National Natural Science Foundation of China (Grant Nos. 10904061, 11034005, 61475070, 11474157, and 11321063), the State Key Program for Basic Research from the Ministry of Science and Technology of China (Grant Nos. 2012CB921502), and

Reuse of AIP Publishing content is subject to the terms at: https://publishing.aip.org/authors/rights-and-permissions. Download to IP: 210.28.138.101 On: Wed, 09 Nov 2016 09:23:29

China Scholarship Council. Work at UC Davis was supported in part by the National Science Foundation Grant No. ECCS-0725902. Work at Lawrence Livermore National Laboratory was performed under the auspices of the U.S. Department of Energy by Lawrence Livermore National Laboratory under Contract DE-AC52-07NA27344.

[1] R. A. de Groot, F. M. Mueller, P. G. van Engen, and K. H. J. Buschow, Phys. Rev. Lett. **50**, 2024 (1983).
[2] Y. Ji, G. J. Strijkers, F. Y. Yang, C. L. Chien, J. M. Byers, A. Anguelouch, G. Xiao, and A. Gupta, Phys. Rev. Lett. **86**, 5585 (2001).
[3] C. Hordequin, D. Ristoiu, L. Ranno, and J. Pierre, Eur. Phys. J. B **16**, 287 (2000); I. Žutić, J. Fabian, and S. Das Sarma, Rev. Mod. Phys. **76**, 323 (2004).
[4] M. Julliére, Phys. Lett. A **54**, 225 (1975).
[5] P. Larson, S. D. Mahanti, and M. G. Kanatzidis, Phys. Rev. B **62**, 12754 (2000).
[6] R. W. G. Wyckoff, *Crystal Structures*, 2nd ed. (John Wiley & Sons, 1963), Vol. 1.
[7] W. Huang, X. Wang, X. Chen, W. Lu, L. Damewood, and C. Y. Fong, J. Magn. Magn. Mater. **377**, 252 (2015).
[8] L. Damewood, B. Busemeyer, M. Shaughnessy, C. Y. Fong, L. H. Yang, and C. Felser, Phys. Rev. B **91**, 064409 (2015).
[9] J. E. Pask, L. H. Yang, C. Y. Fong, W. E. Pickett, and S. Dag, Phys. Rev. B **67**, 224420 (2003).
[10] H. Akinaga, T. Manago, and M. Shirai, Jpn. J. Appl. Phys. **39**, L1118 (2000).
[11] S. Wurmehl, G. H. Fecher, V. Kesenofontov, F. Casper, U. Stumn, C. Felser, H. Lin, and Y. Hwu, J. Appl. Phys. **99**, 08J103 (2006).
[12] M. Shaughnessy, L. Damewood, C. Y. Fong, L. H. Yang, and C. Felser, J. Appl. Phys. **113**, 043709 (2013).
[13] G. Kresse and J. Furthmüller, Phys. Rev. B **54**, 11169 (1996); Computational Materials Science **6**, 15 (1996).
[14] G. Kresse and J. Hafner, Phys. Rev. B **49**, 14251 (1994); **47**, 558 (1993).
[15] P. E. Blöchl, Phys. Rev. B **50**, 17953 (1994).
[16] J. P. Perdew, K. Burke, and M. Ernzerhof, Phys. Rev. Lett. **77**, 3865 (1996).
[17] Damewood *et al.*, in preparation.

Reuse of AIP Publishing content is subject to the terms at: https://publishing.aip.org/authors/rights-and-permissions. Download to IP: 210.28.138.101 On: Wed, 09 Nov 2016 09:23:29